lubricants

MDPI

Article

A Generalised Method for Friction Optimisation of Surface Textured Seals by Machine Learning

Markus Brase *,†, Jonathan Binder †, Mirco Jonkeren and Matthias Wangenheim

Institute of Dynamics and Vibration Research, Leibniz Universität Hannover, 30823 Garbsen, Germany; jonkeren@ids.uni-hannover.de (M.J.); wangenheim@ids.uni-hannover.de (M.W.)

* Correspondence: brase@ids.uni-hannover.de

† These authors contributed equally to this work.

Abstract: Friction behaviour is an important characteristic of dynamic seals. Surface texturing is an effective method to control the friction level without the need to change materials or lubricants. However, it is difficult to put the manual prediction of optimal friction reducing textures as a function of operating conditions into practice. Therefore, in this paper, we use machine learning techniques for the prediction of optimal texture parameters for friction optimisation. The application of pneumatic piston seals serves as an illustrative example to demonstrate the machine learning method and results. The analyses of this work are based on experimentally determined data of surface texture parameters, defined by the dimple diameter, distance, and depth. Furthermore friction data between the seal and the pneumatic cylinder are measured in different friction regimes from boundary over mixed up to hydrodynamic lubrication. A particular innovation of this work is the definition of a generalised method that guides the entire machine learning process from raw data acquisition to model prediction, without committing to only a few learning algorithms. A large number of 26 regression learning algorithms are used to build machine learning models through supervised learning to evaluate the suitability of different models in the specific application context. In order to select the best model, mathematical metrics and tribological relationships, like Stribeck curves, are applied and compared with each other. The resulting model is utilised in the subsequent friction optimisation step, in which optimal surface texture parameter combinations with the lowest friction coefficients are predicted over a defined interval of relative velocities. Finally, the friction behaviour is evaluated in the context of the model and optimal value combinations of the surface texture parameters are identified for different lubrication conditions.

Keywords: supervised learning; regression techniques; surface texturing; dynamic seals

Citation: Brase, M.; Binder, J.; Jonkeren, M.; Wangenheim, M. A Generalised Method for Friction Optimisation of Surface Textured Seals by Machine Learning. *Lubricants* **2024**, *12*, 20. https://doi.org/10.3390/lubricants12010020

Received: 2 November 2023
Revised: 14 December 2023
Accepted: 26 December 2023
Published: 9 January 2024

1. Introduction

Friction is defined as the force of resistance acting between the contact surfaces of bodies in relative motion [1]. In total, about 20% of global energy losses are due to overcoming friction [2]. Therefore, low friction is targeted in many technical systems such as seals or bearings. In order to reduce friction in tribological systems, it is necessary to understand the individual factors that influence friction and to develop appropriate strategies to minimise the friction [1].

On the one hand, material properties, such as the crystal structure [3], hardness [4,5], elastic and shear modulus [6,7], grain size [8,9], and surface energy [10,11] of the contacting materials affect the frictional behaviour. On the other hand, the operational conditions, such as the normal loads [12,13], sliding velocities [14,15], environmental conditions [16,17], temperatures [18], and lubricants [19], have a major influence on the tribological behaviour. Of particular relevance are surface coatings or modifications of the surface topographies [20], which both can contribute significantly to the friction behaviour. Surface modifications involve techniques that artificially alter the structures of the solid surfaces through defined

properties. This involves texturing the surface either by adding material to create protrusions or by removing material, displacing material and using self-moulding techniques to create dimples [21,22]. Surface modifications can be achieved by changing the surface roughnesses [23], textures [24], or a combination of both [25].

In order to reduce the friction of a tribological system, the performance of the lubricant can be improved [26], the lubricant feeding conditions can be adjusted and optimised [27], special materials and coatings can be used [28], operational conditions can be modified [29], geometries can be optimised [30], and the contact surfaces can be modified [24]. In addition, it is possible to combine different processes, such as surface texturing and surface coating [31,32]. Within this work, surface textured seals are analysed as an example application. The textures, applied to the seal surfaces, are defined by the dimple diameter, dimple distance, and dimple depth. This is why, surface modifications, specifically surface texturing, are of particular interest. Surface textures have been demonstrated to positively influence friction and wear under both dry friction conditions [33] as well as boundary [34], mixed [35], elastohydrodyamic [36], and full-film hydrodynamic lubrication conditions [37]. Surface textures exhibit different beneficial effects on friction, depending on the lubrication regime. The textures can reduce the real area of contact [38], trap wear particles [39], accelerate the formation of tribolayers [40], store lubricant [41], draw additional lubricant into the contact area [25], build-up additional hydrodynamic pressure [42], and locally increase the fluid film height [43]. However, the mechanisms through which the textured surface parameters affect the friction performance, such as the texture density or depth, are still not fully understood and require further investigation [44]. Surface texturing is highly application dependent and must be evaluated for each tribological system and lubrication regime. Furthermore, the possible number of parameters for the surface texture design is immense [45].

In this respect, machine learning is a powerful tool to predict application-dependent optimum texture parameters and to overcome or reduce time consuming and expensive trial-and-error approaches [46]. The advantages and potentials of machine learning techniques lie in the handling of high-dimensional problems and the ability to adapt models to changing conditions with reasonable effort [47], even if the physics behind the tribological system is not fully understood [48]. According to the systematic reviews by Marian et al. [47] and Paturi et al. [48], the number of tribology papers successfully investigating and applying machine learning techniques is increasing exponentially. For example, about 46% of the 330 papers evaluated were written between 2018 and 2022 [48]. In addition, around 76% of the 127 articles quantitatively analysed by Marian et al. were based on experimentally collected data. The learning algorithm used in about three quarters of the papers was a neural network category algorithm, making them overrepresented in the tribological context [47]. So, it is noticeable that authors tend to focus on a few learning algorithms at an early stage. However, other algorithms can also show comparable or even better results, as presented in Section 5.2, so these should not be excluded from the analysis from the outset. Based on the "no free lunch" theorem, it is only possible to know exactly which model is the most suitable for the present application and data, if it has been trained and tested [49]. As shown in Section 5.2, it is possible that not only one algorithm shows good results, but that there are several suitable algorithms. Also, the numerous application examples cited by Marian et al. [47] show that there is no universally applicable learning algorithm for tribological problems. According to the "no free lunch" theorem, the selection of a suitable learning algorithm must, therefore, always be made individually for the prevailing application and is a challenge in the development of models in machine learning [50]. It is, therefore, necessary to optimise the selection of texturing parameters based on data from experiments or simulations, using several machine learning (ML) algorithms.

Within this paper, the MATLAB Statistics and Machine Learning Toolbox® is utilised to build regression models. The toolbox contains 26 learning algorithms from seven categories. As an innovation, all of them are taken into account during the study to make an informed

model selection based on trained and tested models with various evaluation metrics. The aim is to be able to quickly identify the best of the 26 models, without having to perform complex processes such as hyperparameter optimisation of single models, and thus enable users who are not experts in machine learning to apply the ML methods. For this purpose, a generalised method is explained on the basis of the selected aspects of the tribological example application of surface textured pneumatic piston seals. This application serves as an illustrative example. However, the methodology can also be applied to other surface textured systems, such as metallic components or rubber parts.

2. Generalised Method for Machine Learning Model Generation and Application

The procedure acquired in this paper for developing machine learning models in the context of tribological applications is shown in the flowchart below, see Figure 1. Although this is not a universal and valid method in general, the flowchart shows the most common methods, provided in the literature, that can be used.

Figure 1. Flowchart of a generalised machine learning development method using standard machine learning techniques. The illustration shows an overview of the individual steps, which are briefly explained in the following chapters.

The quality of the recorded data is of great importance, so careful data acquisition must first be ensured, indicated by the grey step of the flowchart. This step is explained

more in detail in Section 3 for the example application of surface textured pneumatic piston seals. Based on this, data analysis and data preparation are necessary, indicated by the blue steps of the flowchart. Using the prepared data, model building is performed, see the first orange step of the flowchart. Data analysis, data preparation, and model building are described in Section 4.

The best model is selected using mathematical performance ratios and partial dependence plots in the context of tribological relationships, like Stribeck curves, indicated by the second orange step of the flowchart, which is explained more in detail in Section 5. In addition, this chapter contains the application of the generated model for the selection of the optimal surface texture parameters, according to the purple steps of the flowchart, and the preliminary examination of the friction results, depicted by the yellow steps. Based on the green step of the flowchart, the tribological context of the friction results are discussed in Section 6.

3. Friction and Seal Surface Texture Data Acquisition

Data acquisition is a process that leads to pre-processed measurement data, highlighted as the grey step in the flowchart, shown in Figure 1. Within this step, data on friction values and surface texture parameters of dynamic pneumatic piston seals are measured, which together form the basis of the machine learning model.

3.1. Friction Measurements

The objective of the experimental testing procedure is to measure the friction forces between surface textured pneumatic piston seals and a static pneumatic cylinder tube by utilising a linear test rig, explained in Figure 2. The tribotechnical system considered to record the friction forces consists of a pneumatic piston seal and a pneumatic cylinder tube, see Figure 2b.

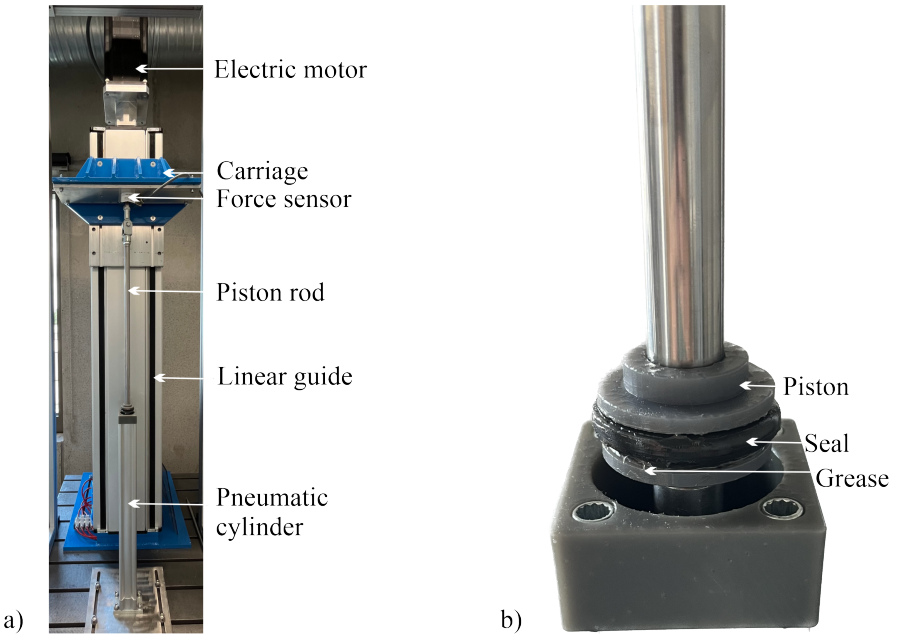

Figure 2. (**a**) Universal linear test rig. The carriage, connected to the linear guide, is driven by an electric motor. The piston rod is connected to the carriage by a force sensor. The piston rod is linked to the piston, in which the seal is installed. The seal can thus be moved relative to the static pneumatic cylinder tube at the set velocity. (**b**) Tribotechnical System. A detailed view of the piston and seal reveals the tribotechnical system. It consists of the base body (pneumatic piston seal) and the counter body (pneumatic cylinder tube). The intermediate medium is a lubricating grease.

The nominal external diameter of the seal and internal diameter of the pneumatic cylinder are equal to 40 mm. The material of the seals, which are manufactured by texturing

during moulding (TDM) [51], is a fluoroelastomer with a Shore hardness of 80 A (FKM80A). The pneumatic cylinder tube is made of anodised aluminium. Throughout the test procedure, the same grease is used as in the interfacial medium [52]. An important challenge during the measurements is the creation of a lubricating film that ensures reproducible friction force measurements. Care must be taken to ensure that a consistent amount of lubricant is present inside the pneumatic cylinder for each seal that is measured. This was achieved by applying a constant mass of lubricant to the seals, cleaning the cylinder between the measurements of two seals, and applying a constant mass of lubricant to the cylinder itself. It has also been found that it is beneficial to measure friction on one seal, starting at the highest velocity and decreasing towards the lowest velocity. The reason for this is that the lubricant film is thickest at the highest velocities and is more easily dissolved than built up during the test procedure, which means that conditioning runs between velocities can be reduced. All of the experiments were performed at an ambient temperature of 20 °C. In contrast to the real technical application of a pneumatically driven actuator, the relative movement between the seal and the pneumatic cylinder was applied by the linear guide of the test rig. Within the entire test procedure, the pneumatic cylinder was depressurised. Each seal was tested at 19 test speeds ranging from 1 mm/s to 500 mm/s, moving at a predefined trapezoidal speed profile, see Figure 3a. The distance to be driven was selected between 15 mm and 450 mm depending on the velocity of the seal. For each measurement, the piston was moved in two directions from the start position to the end position and back again. This corresponded to one test cycle. A total of 12 cycles were performed for each test speed and seal. This resulted in 228 friction measurement cycles per seal, consisting of 228 downstrokes and 228 upstrokes.

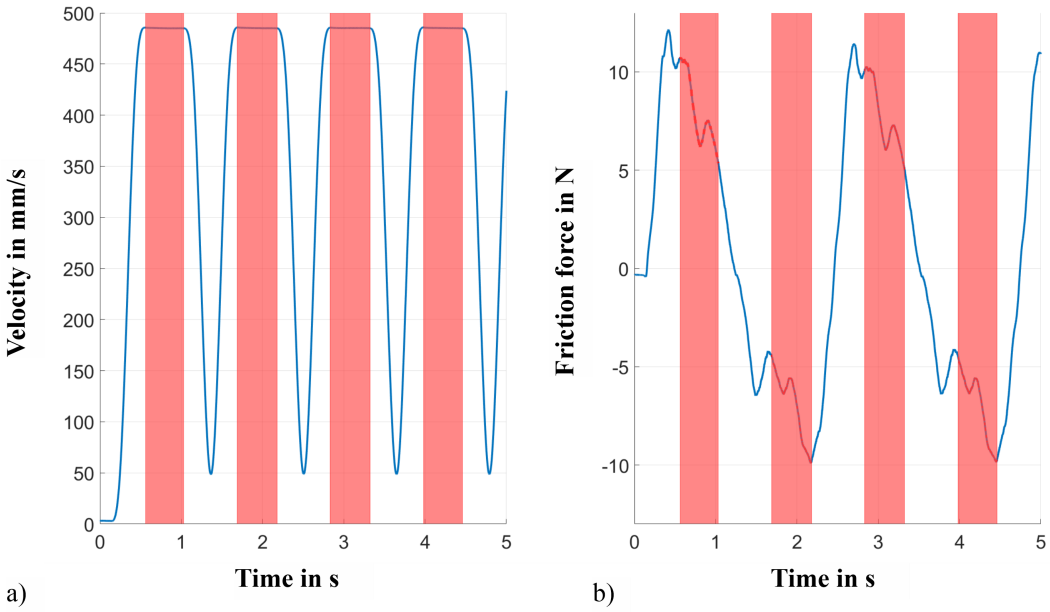

Figure 3. (**a**) Trapezoidal velocity profile of the test rig. Within the stationary area of constant velocity, marked in red, the mean value of the friction force is determined, which is used for further analyses. (**b**) Friction force as a function of time. Positive values of friction indicate the downstroke of the test rig, while negative values indicate the upstroke. The friction force signal shows a bumpy curve, as the friction distance at the higher speeds is not sufficient to generate a constant value in the friction force signal.

A conditioning run is carried out before the 12 measured cycles in order to adjust the tribological system and, in particular, the lubricant film height to the current velocity. The temperature in the contact between the seal and cylinder was not recorded. However, as the measurement results were within the 6 sigma interval and no systematic increase or decrease in the friction characteristics could be identified over the number of cycles, a temperature change in the contact was regarded to be negligible for friction evaluation. The quasi-stationary friction force signal was evaluated from the friction signal at time intervals where the velocity was stationary, see Figure 3b. To calculate the corresponding friction coefficients associated with the friction forces, which were further processed in the machine learning (ML) model, the required normal forces were provided by static FE simulations of the contact pressure distribution between seal and cylinder. The FE model, which uses a hyperelastic material model, was not the focus of this work, and was, therefore, not described in detail.

3.2. Seal Surface Texture Measurements

In contrast with other studies, the machine learning model does not use nominal texture parameters, but rather the real texture parameters of the pneumatic piston seals that are measured. The surface analyses of the seals were based on 3D microscope measurements, which were recorded using the method of focus variation. The collected data were exported as cartesian xyz data points, see Figure 4a. Based on these data points, the surface was visualised in two different areas—the textured (blue/green) and untextured (yellow/orange) areas, see Figure 4b.

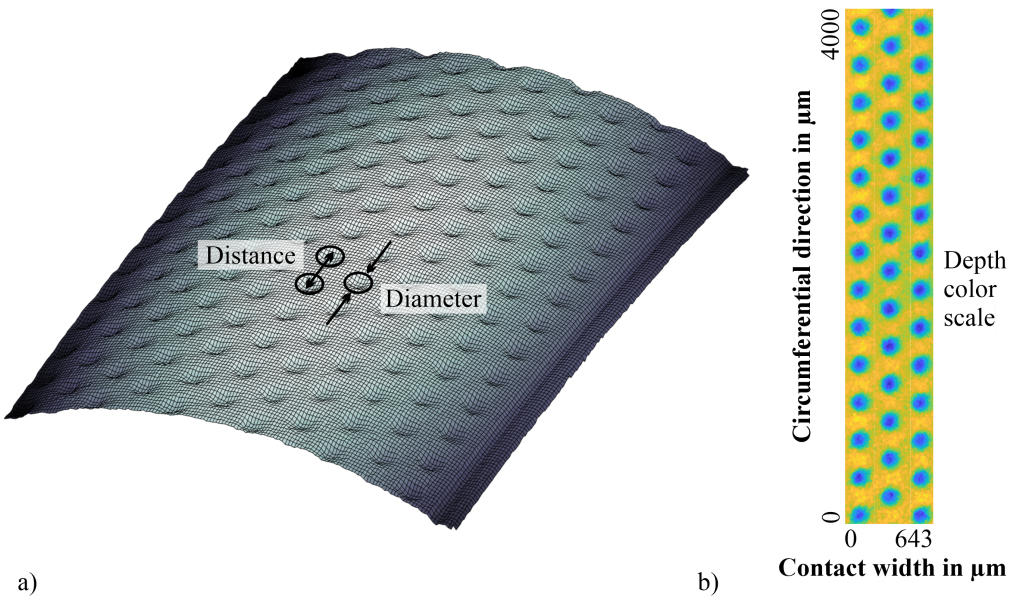

Figure 4. (**a**) Microscope surface scan of a textured seal (4 × 4 mm). The circles enclose the triangular arranged circular dimples. The texture parameters of dimple diameter and dimple distance are defined by the arrows. (**b**) Dimple depth information of the microscope scan. The yellow and orange areas represent the untextured area of the seal surface, while the green and blue areas represent the dimples with their depth.

On basis of the FE simulations already mentioned in Section 3.1, the contact width between the seal and pneumatic cylinder tube is calculated, from which the effective contact area is determined. The texture density, shown in Table 1, therefore only corresponds to the density in effective contact between the seal and cylinder and neglects the textured seal area that is not in contact, as it is tribologically irrelevant. The surface textures are defined by the dimple diameter, distance, and depth. They have a basic circular shape and are arranged in a triangular pattern. The diameter of the dimples is determined using circular approximations of the green/blue data points. The dimple depth is the mean value

of all data points within these approximated circles. In addition, the distance between the dimples is calculated using the centre points of the approximated circles. This is not only done for one individual dimple, but for the entire number of dimples, which are positioned within the measuring area of 4×4 mm and the simulated contact width of $l = 643$ µm of the seal. The corresponding number of evaluated dimples is specified in Table 1. The related dimple parameters are determined as the mean values of the given number of individual measurements. The real texturing density is the ratio of the textured to untextured area of the analysed seal surface. Because of process tolerances that occur during the laser and vulcanisation process of the seals, odd values can be seen in Table 1.

The general seal dimensions, more precisely the inner and outer diameters of the seals and their deviation from nominal values, were not measured and considered, which is discussed in Section 6 and mentioned in the outlook.

Table 1. Real seal surface texture parameters. The values are the mean value of the specified number of analysed dimples within the simulated contact width of the seal.

Seal No.	Diameter in µm	Distance in µm	Depth in µm	Texture Density in %	Number of Analysed Dimples
1	-	-	-	-	-
2	97	195	7.9	20.4	58
3	96	243	8.6	15.3	46
4	100	244	11.4	15.8	43
5	149	244	14.5	34.3	46
6	143	292	12.9	25.2	37
7	147	294	19.3	26.8	37
8	149	294	24.8	27.2	37
9	196	293	23.6	45.0	37
10	199	390	23.3	21.9	28
11	147	293	19.1	26.3	37

4. Data Analysis, Data Preparation, and Model Development

The machine learning algorithms discussed in this paper are classified as supervised learning. Within this category, regression algorithms were used, which deal with numerical continuous output values. The training of the algorithms was conducted with a known set of input data and known responses, which are the data collected in Section 3.1. The data analysis, data preparation, and model development were guided by the method shown in Figure 1. For the development of machine learning models, high data quality is an essential requirement. This started with a comprehensive analysis of the available data to assess their quality, which included an examination of its structural characteristics and properties (data analysis). This understanding subsequently facilitated the preparation of the available data with the aim of improving its quality, as well as its transformation into the desired format (data preparation) [50,53]. Afterwards, model development began.

In order to be able to evaluate the data quality as part of the data analysis, a data quality report (DQR) according to [50] was generated in this study for the available measurement data. The report took the total number of numerical values, data completeness, cardinality, minimum and maximum values, first and third quartiles, median and arithmetic mean, and the standard deviation into account, which is shown in Table A1 of the Appendix A. It was found that there were no missing values in the features studied, that the data had a uniform character, and that there were no irregularities in the other indicators of the data quality report. Interquartile ranges (IQRs) were calculated to identify individual data points that represent mathematical outliers [53,54], which require a more detailed and individual examination. Based on this examination, it becomes apparent that the identified outliers were only default values for the test series or the texture parameters, specifically friction values, that can be evaluated as being feasible with the help of the physical relationship of the Stribeck curve. The sliding velocity can be used as an illustrative example. In Figure 5 it is visible that the sliding velocity was not sampled uniformly. The lower velocities were

sampled more finely than the higher velocities. As a result, the higher values were marked as mathematical outliers, although they were not physically outliers. Therefore, all these data points were used for further analysis. The IQR calculated for the features can be found in Figure A1 of the Appendix A.

In the context of data preparation, dimensionality is particularly important. Data sets with high dimensionality lead to increased complexity, computational effort, and the risk of overfitting [55,56]. For this reason, it is more useful to have many data points for each feature, but not a larger number of features, because only features with a high significance add value to the model and its accuracy [56].

In order to reduce the number of features while preserving the most relevant information, principal component analysis (PCA) is used as a feature extraction method to assess dimensionality. As this is a requirement for PCA, the existing data sets are standardised so that the values of each feature are within the interval $[-1; 1]$ and have an arithmetic mean of zero as well as a standard deviation of one. According to the first principal component, the feature of sliding velocity has the greatest influence on the coefficient of friction, since it explains 85.34% of the variance. According to the second principal component, the texture parameters dimple diameter, dimple distance and dimple depth have the greatest influence, because they explain 13.40% of the variance. As a result, the analysis shows that the first two principal components already explain 98.74% of the variance. The features that have been examined are shown in Table 2. Based on the principal component analysis, features with little influence on the variance of the original data can be removed.

Table 2. Coefficients of the first two principal components (PC 1 and PC 2) for the examined features. The remaining features after PCA are highlighted in bold letters. Cycle and direction of motion are removed.

Feature	**Sliding Velocity**	**Cycle**	**Direction of Motion**	**Dimple Diameter**	**Dimple Distance**	**Dimple Depth**	**Texture Density**
PC 1 (85.34%)	1.00	0.00	0.00	0.00	0.00	0.00	0.00
PC 2 (13.40%)	0.00	0.00	0.00	0.55	0.83	0.09	0.00

The model is built using recursive feature elimination (RFE) according to the cross-validation (CV) procedure. For this purpose, the training data is divided into a training set and a test set. In this model development, 10% of the training data was used as test data. To ensure that the quality of the generated model does not depend on the division of the training data into training and validation sets, a variant of cross-validation called k-fold cross-validation (KFCV) is used [53,56]. For model development, the training data is divided into k subsets. In this study the cross-validation procedure is performed with $k = 5$ or $k = 10$ subsets, depending on the number of records.

During the RFE process, features are eliminated iterative as part of model development, which is outlined in Section 5.2. The minor influence of the cycle and the direction of motion, as already observed in the PCA (see Table 2), can be confirmed. Hence, these features are eliminated. The friction coefficients per seal and velocity are averaged over the measured up and down cycles, which is possible due to the symmetry of the seal, so that the up and downstroke force is nearly identical. The feature texture density is not removed from the training data, since it is directly related to the dimple distance and diameter. This reduces the number of data sets to $N = 190$ (10 surface textured seals and 19 tested sliding velocities), leaving $M = 5$ features.

A total of 26 learning algorithms, shown in Table 3, are used for model development using MATLAB Statistics and Machine Learning Toolbox®.

Table 3. Summary of all algorithms studied by category: Supervised Learning—Regression. Algorithm 16, which is chosen to build the best model within the prevailing application, is highlighted by underlining, compare also Table 4. The four colored algorithms correspond to the curves of Figure 6.

Category	No.	Algorithm
Linear Regression Models	1	Linear
	2	Interactions Linear
	3	Robust Linear
	4	Stepwise Linear
Regression Trees	5	Fine Tree
	6	Medium Tree
	7	Coarse Tree
Support Vector Machines	8	Linear SVM
	9	Quadratic SVM
	10	Cubic SVM
	11	Fine Gaussian SVM
	12	Medium Gaussian SVM
	13	Coarse Gaussian SVM
Gaussian Process Regression Models	14	Squared Exponential
	15	Matern 5/2
	16	Exponential
	17	Rational Quadric
Kernel Approximation Models	18	SVM Kernel
	19	Least Squares Kernel Regression
Ensembles of Trees	20	Boosted Trees
	21	Bagged Trees
Neural Networks	22	Narrow Neural Network
	23	Medium Neural Network
	24	Wide Neural Network
	25	Bilayered Neural Network
	26	Trilayered Neural Network

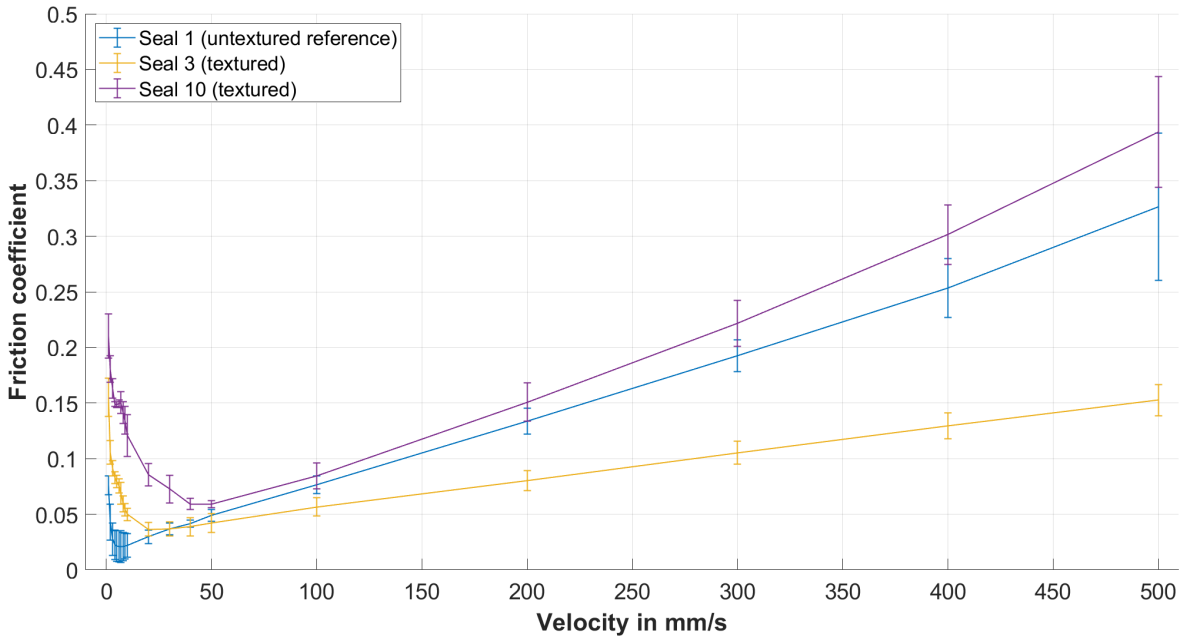

Figure 5. Stribeck curves from two different surface texture parameters, compared with the untextured reference. The single data points were provided with error bars.

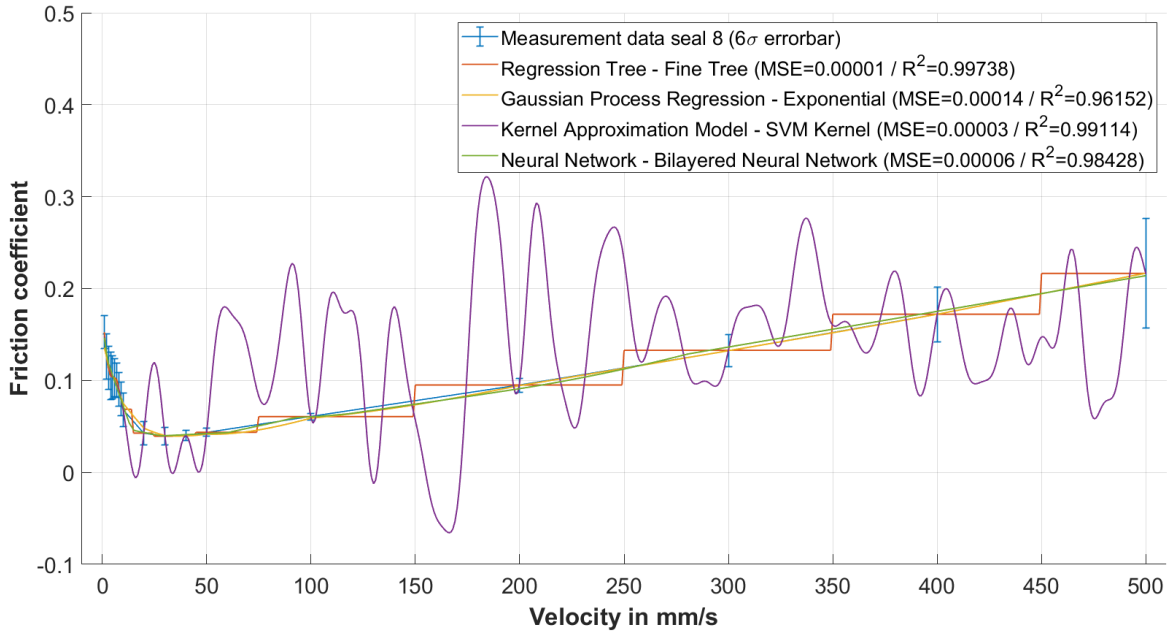

Figure 6. Pre-Comparison of the predicted Stribeck curves, based on the best algorithm each within the four best model categories according to the performance indices using seal sample 8 as an example. The curves are only based on the first model epoch, considering the maximum dataset before RFE. The individual data of the first epoch are specified in Table A2. The results of the last epoch after RFE can be found in Table 4.

Table 4. Comparison of the last epoch of the four algorithms, shown in Figure 6. The features cycle and direction of movement were already removed after recursive feature elimination (RFE), resulting in an implementation with averaged friction coefficients as described above. Only these four algorithms were evaluated up to the last epoch. The other algorithms from Table 3 were discarded due to poor metrics in the first epoch.

No.	Algorithm (Category)	*MSE*	R^2
5	Fine Tree (Regression Trees)	0.00050	0.78870
16	**Exponential (Gaussian Progress Regression Models)**	**0.00009**	**0.96077**
18	SVM Kernel (Kernel Approximation Models)	0.00320	−0.4098
25	Bilayered Neural Network (Neural Networks)	0.00070	0.68924

5. Friction Measurement Results and Machine Learning Model

5.1. Preliminary Examination of the Friction Results

From the friction coefficients per seal and sliding velocities described in Section 3.1, Stribeck curves were generated for the qualitative preliminary investigation. According to the principal component analysis (PCA) of Section 4, the features direction of the motion and cycle were not significant. Therefore, the friction coefficients per seal and velocity were averaged. Figure 5 shows the exemplary Stribeck curves of textured seals 3 and 10 compared with the untextured reference seal 1, compared with Table 1.

The curves represent the average friction coefficients per seal, while the error bars mark the 6 sigma interval at the test velocity, to obtain 99.7% as the confidence interval. It can be seen that the textured seals had higher friction coefficients in the boundary and mixed friction regime than the untextured reference. In addition, the area of mixed friction was more pronounced and extended over a larger velocity interval depending on the texture parameters. On the other hand, the Stribeck curve of seal 3 shows that texturing could lead to lower friction coefficients in the hydrodynamic friction region. The texture parameters of seal 3 were proven to be advantageous in a direct comparison with the textures of the 9 other textured seals, as the associated Stribeck curve has the lowest coefficients of

friction in the hydrodynamic friction regime due to a lower slope. In contrast, the texture parameters of seal 10 resulted in high friction coefficients in all of the friction regimes. This shows that surface texturing did not automatically lead to an improved friction behaviour. In addition, the qualitative preliminary examination of the collected measurement data indicated the need for a model to identify optimal and discrete texture parameters and to fathom tribological relationships in a factual context.

5.2. Machine Learning Model

The model was built using the MATLAB Statistics and Machine Learning Toolbox® by recursive feature elimination according to the *k*-fold cross-validation method, see Section 4. The training data were based on the measured friction and surface data of 10 textured pneumatic piston seals, whose texture was characterised by dimples with a circular basic shape in a triangular pattern, compared with Section 3.2. The maximum dataset consisted of $N = 4560$ records (228 + 228 piston strokes multiplied with 10 textured seals) and $M = 7$ features according to Table 2, each with an associated friction coefficient output. In the first model generation step, one model was generated for each of the 26 learning algorithms specified in Table 3 using the MATLAB toolbox. In this process, $k = 10$ folds were used in the *k*-fold cross validation (KFCV). Furthermore, 10% of the records were separated as the test dataset, from which the mathematical evaluation metrics MSE and R^2 [53,57] were calculated. As an example, Figure 6 shows different Stribeck curves, predicted by four different algorithms based on seal 8, in comparison with the measured friction values of seal 8. The related performance indices of the four models are summarised in the legend. The figure clarifies that the evaluation of the models using solely mathematical evaluation metrics was inadequate. The Regression Tree and Kernel Approximation models showed the best performance indices, but were unable to reproduce the known dependency between the velocity and friction coefficient as a Stribeck curve with the available experimental data. In particular, the Kernel Approximation Model showed a clear overfitting. Only at discrete test velocities could the friction coefficients be accurately predicted. In addition to the performance indices, it was advisable to evaluate the models on the basis of known partial dependencies, which represented the dependence between the target response, friction value, and at least one feature. The Gaussian Process Regression and Neural Network models not only showed good performance indices, but also reproduced the partial dependence between velocity and friction coefficient as a Stribeck curve according to Figure 6. Especially in case of non-parametric models, a priori selection of learning algorithms was not advisable, as it was difficult to estimate how they reacted to the training data. As in Figure 6, the overfitted kernel approximation model showed similar correlations in other partial dependencies, which could be visualised using partial dependence plots (PDP). For example, the correlation between the dimple diameter and friction coefficient was unknown, but a strongly fluctuating correlation with many deflections was not expected from a tribological point of view.

The recursive feature elimination within the first model generation showed that the features direction of movement and cycle were not significant. The method thus confirmed the results of the principal component analysis of Section 4. The final model generation was, therefore, performed with the averaged friction coefficients, as described in Section 4. The training data consisted of $N = 190$ records and $M = 5$ features. For model building, $k = 5$ folds were used. Further, 10% of the records were separated as the test dataset in order to be able to determine the performance indices on the basis of unknown data. The comparison of the last epoch of the performance indices of the four algorithms, shown in Figure 6, is provided in Table 4. It is clear that the neural network, which had both good mathematical metrics and a good representation of tribology in the form of the Stribeck curve, had poor MSE and R^2 values in the last epoch. Therefore, throughout the course of model development and evaluation, an exponential Gaussian Process Regression model, underlined in Table 3, with the following features emerged as the best model in the

applications context: velocity, dimple diameter, dimple distance, dimple depth, and real texture density inside the contact area.

The GPR model reveals the following performance indices: $MSE = 0.00009$ and $R^2 = 0.96077$. The performance indices of the model with a reduced number of features of $M = 5$ were almost identical to those of the maximum dataset of the first model generation. The MSE even improved slightly. The friction coefficients could thus be predicted with a high degree of certainty for discrete texture parameters at different sliding velocities. As shown previously, the model was able to reproduce the known dependency friction velocity as a Stribeck curve. Further evaluation of the model performance, e.g., using a residual plot, showed no anomalies that would indicate a poor model fit [57].

To identify optimal texturing parameters, the selected machine learning model was used to predict friction coefficients for discrete combinations of feature values within the intervals of the training data. Thus, there was no prediction by extrapolation. The generated Stribeck curves could be used to evaluate the tribological behaviour of the textured seals within different friction regimes. Figure 7 shows the prediction interval (grey area), in which the model could create predictions for the feature intervals specified in Table 5, compared with the mean friction curve of the untextured reference seal 1. It can be seen that there was no texture parameter combination, based on the model, that led to lower friction coefficients in the boundary and mixed friction regime.

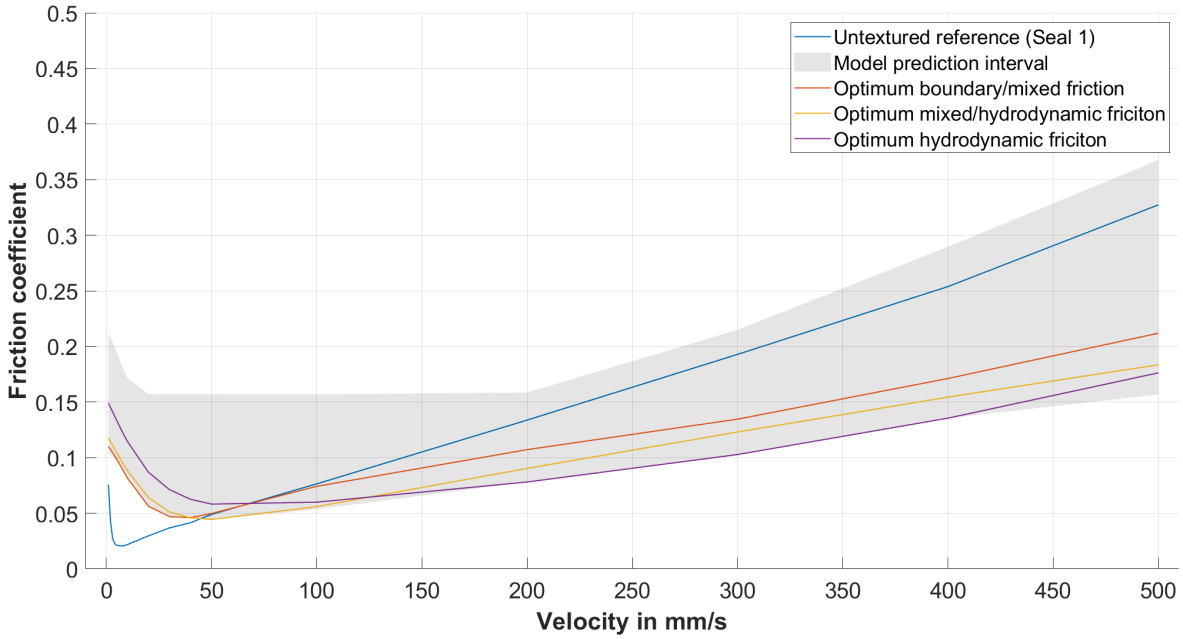

Figure 7. Model evaluation: comparison of the untextured reference seal 1 to the model prediction interval (grey area) and Stribeck curves, predicted by the model, of the identified optimum texture parameters for each friction regime.

Table 5. Feature intervals used for the machine learning model evaluation.

Feature	Unit	Min.	Max.	Resolution
Velocity	mm/s	1	500	19 values
Diameter	µm	95	205	5
Distance	µm	190	400	10
Depth	µm	5	30	1
Texture density	%	15	45	1

No texture emerged as a global optimum from the parameter study carried out. Three predicted Stribeck curves could be identified, each of which could be considered as an optimum in one of the friction states. The corresponding texture parameters are

summarised in Table 6. From the model prediction, it can be seen that all three texture parameters led to lower friction coefficients in the hydrodynamic friction region compared with the untextured reference. However, low friction coefficients in the hydrodynamic friction regime were at the expense of increased friction coefficients in the boundary and mixed friction regions. In addition, the transition to hydrodynamic friction was shifted to higher speeds, so that boundary and mixed friction were more pronounced over a larger velocity interval. These results were consistent with the preliminary examination, as explained in Section 5.1.

Table 6. Optimal texture parameters for each friction regime according to the machine learning model prediction. Friction increase and friction reduction are related to the untextured reference seal 1. The data are based on the values from the graphs of Figure 7, taking into account the discrete values, as specified in Table 5.

No.	Optimum	Diameter in µm	Distance in µm	Depth in µm	Texture Density in %	Max. Friction Increase (Velocity)	Max. Friction Reduction (Velocity)
1	Boundary/Mixed friction	145	290	13	25	362% (5 mm/s)	35% (500 mm/s)
2	Mixed/Hydrodyn. friction	95	240	9	16	390% (5 mm/s)	44% (500 mm/s)
3	Hydrodyn. friction	145	290	19	26	526% (5 mm/s)	47 % (500 mm/s)

The optimum texture in the transition zone from mixed friction to hydrodynamic friction No. 2 from Table 6 can be identified as a compromise between Nos. 1 and 3. At the maximum velocity of 500 mm/s, the maximum predicted friction coefficient reduction was approximately 44%. In addition, the predicted friction coefficient of $\mu = 0.044$ at a velocity of 50 mm/s for these texture parameters was the lowest within the entire predictions of the machine learning model.

As mentioned above, the chosen textures on which the model was based were associated with a significant increase in the friction coefficients in the boundary and mixed friction regions. As can be seen in Table 6, there was a maximum increase in the friction coefficient of 526% at a low speed of 5 mm/s. So, it became clear that the improvement in the frictional behaviour strongly depended on the surface texture and especially on the operational conditions such as the sliding velocity of the seal.

6. Tribological Discussion of the Machine Learning Model Results

The Gaussian process regression (GPR) model, which was the most suitable model for the present application and the existing data in a tribological context, reproduced the property of a Stribeck curve, as explained in Section 5. Based on this property and the mathematically metric values specified in Section 5.2, the validity of the model could be assumed. As described, suitable surface textures significantly reduced friction in a hydrodynamic lubrication regime. However, an increase in friction was observed in the boundary and mixed friction regions.

There are several possible reasons for this behaviour, which is contrary to most of the literature, where the dimples showed a reduction in friction over nearly the entire range of operational conditions, e.g., due to their improved micro-hydrodynamic pressure build up or their lubricant storage effect [21,37,58–62]. In fact, however, the dimples could not only serve as a source of lubricant and thus support hydrodynamic film formation, but also as a sink in the event of mixed friction or insufficient lubrication. At low sliding velocities or during idle periods, lubricant collected in and around the dimples, causing the roughnesses of the untextured areas of the seal to be in contact with the roughnesses of the pneumatic cylinder tube surface for a longer period of time, which increased the frictional force in the mixed friction area. This effect increased with the viscosity of the lubricant, which was consistent with the present friction measurements, as a grease with a higher viscosity was

used. Untextured seals, therefore, have the advantage that less lubricant was required to separate the contact surfaces in this lubrication condition [63].

Another possibility for increasing friction at low speeds, where the surfaces were not completely separated from each other as in the hydrodynamic lubrication state, was based on the texturing during moulding (TDM) manufacturing method of the seals. During production, the negative of the desired dimple texture was applied to the metallic mould by laser ablation. During the vulcanisation process, the texture is directly transferred from the mould to the rubber surface, so that protrusions in the mould became dimples in the seal. The resulting removal of material from the metal mould increased the outer diameter of the seals by an amount equal to the depth of the dimples [51]. This increased the contact pressure between the seal and the pneumatic cylinder tube and thus the friction.

A third possibility for friction increase in the boundary and mixed lubrication regimes was the texture-parameter-dependent wiping effect of the dimples, where at low sliding speeds and, therefore, low film heights, the lubricant was wiped off and the edges of the dimples interlocked with the cylinder surface. The negative contribution of the three effects to friction described above has not yet been studied and quantified in detail, and will be the subject of future research. For this purpose, the tests were to be repeated in a glass cylinder. By recording the dynamic contact between the seal and the glass cylinder with the help of a high-speed camera, lubricant sinks and wiper effects could be detected. In addition, the tests were repeated with different pistons, in which the fit between the inner diameter of the seals and the outer diameter of the pistons was varied. This changed the contact pressure between the seal surface and the internal cylinder surface, allowing manufacturing tolerances to be simulated with defined dimensions. Consequently, their effect on friction could be analysed.

On the other hand, the positive friction-reducing effects of the dimple textures in the hydrodynamic lubrication regime were evident for nearly all of the textured seals analysed in this paper (see the grey area of Figure 7). Textures with extremely large diameters, especially distances above 200 µm and 395 µm, were an exception, due to their inappropriate aspect ratio [64]. This indicates that a positive effect of the dimples was present, but that there was a limit to the positive properties of the dimples with their effect of increasing hydrodynamic pressure build-up for the prevailing specific application of a pneumatic piston seal [25].

It can also be seen that the slope of the Stribeck curve of the textured seals, and therefore the friction coefficient, was generally lower in the hydrodynamic lubrication regime, even though the lubricant was exactly the same in all of the tests. This behaviour could be explained by the advantageous choice of the texturing parameters, which reduced the shear stress inside the lubricant film by increasing the lubrication film thickness due to the increased dimple-induced micro-hydrodynamic pressure build up, which further separated the contacting surfaces [19,65]. In addition, this behaviour was supported by the lubricant storage effect of the dimples, so that sufficient lubricant was provided to separate the surfaces [34,64].

The modelling was exclusively based on the measured values recorded in Section 3. An extension to include measured values such as seal diameter tolerances, temperature, or other disturbing influences could change the results of the methodology in such a way that another of the 26 algorithms analysed was classified as the most suitable for the prevailing application, which will be analysed in future work.

7. Conclusions

The generalised method, presented in this paper, represents essential steps for building regression models through supervised learning, using experimental measured friction and surface texture data as an illustrative example of pneumatic piston seals. In particular, the parallel use of a large number of 26 different machine learning algorithms in the context of an exhaustive search led to good results, even when fundamental correlations in the prevailing data were unknown. The individual steps can be automated, so that the method

is even suitable for identifying trends in ongoing experiments or production processes and for intervening at an early stage if targets are possibly missed. For example, the ML model can be used to identify the operating conditions within the limits of velocity parameters tested, where the surface textures reveal the maximum friction reduction compared with the untextured reference. This is even possible for a texture parameter combination that has not been physically tested.

The approach of this work reveals that machine learning models should be checked as much as possible using different evaluation metrics and should be classified in the specific applications context. Machine learning techniques are particularly treacherous for inexperienced users, as they usually produce good results according to the mathematical performance indicators R^2 and MSE, but may fail to represent the underlying physics, as represented by Stribeck curves. The strength of the generalised method, presented in this paper, lies in its ability to reduce factual relationships to the essential influencing parameters in order to reveal even fundamental physical relationships.

Because it can be fully automated, the method can provide early insights, particularly in tribological testing, that can be directly incorporated into testing procedures and specimen optimisations for the targeted optimisation parameter, such as friction. As Marian et al. pointed out in their systematic review that the automation of data collection and processing could additionally be applied to existing data and completed projects to extend or test relationships and conclusions through machine learning [47]. The generalised method presented in this paper, which is based on common standard machine learning procedures and a large variety of learning algorithms, is a novel and strong tool for the realisation of this approach. The main subjects and findings of the paper are listed below:

1. A novel machine learning methodology is developed to build several ML models and select the most suitable model that reliably predicts optimal surface texture parameters for different operating conditions such as lubrication regimes;
2. Both mathematical metrics and tribological relationships in the form of the Stribeck curve are taken into account to determine the most suitable ML model;
3. Surface textured pneumatic piston seals are used as an example application in this study;
4. Friction measurements of the seals and surface texture measurements of the real parts serve as the basis of data for ML modeling
5. For the example application and the underlying data, a Gaussian process regression (GPR) model has proven to be the best model in terms of mathematical metrics and the tribological representation of the Stribeck curves;
6. Depending on the prevailing friction regimes and surface textures, friction reductions of up to 47%, and friction increases of up to 526% could be identified for the surface textures, compared with an untextured reference surface;
7. The advantage of the method is that a large number of 26 ML models can be compared and the best one selected without having to perform complex processes such as hyperparameter optimisation of individual models, so that a large number of users can use the method without being ML experts.

Author Contributions: conceptualization, M.B. and M.J.; methodology, M.B., J.B. and M.J.; software, J.B.; validation, M.B. and J.B.; formal analysis, M.B. and J.B.; investigation, M.B. and J.B.; resources, M.W.; data curation, M.B. and J.B.; writing—original draft preparation, M.B., J.B. and M.J.; writing—review and editing, M.B., J.B., M.J. and M.W.; visualization, M.B., J.B. and M.J.; supervision, M.B. and M.W.; project administration, M.B. and M.W.; funding acquisition, M.W. All authors have read and agreed to the published version of the manuscript.

Funding: This project has received funding from the European Union's Horizon 2020 research and innovation programme under grant agreement No. 862100.

Institutional Review Board Statement: Not applicable.

Informed Consent Statement: Not applicable.

Data Availability Statement: Dataset available on request from the authors.

Conflicts of Interest: The authors declare no conflict of interest.

Abbreviations

The following abbreviations are used in this manuscript:

CV	Cross validation
DQR	Data quality report
GPR	Gaussian process regression
IQR	Interquartile range
KFCV	K-Fold cross-validation
ML	Machine learning
PCA	Principal component analysis
PDP	Partial dependence plot
RFE	Recursive feature elimination
SPLOM	Scatterplot matrix
SVM	Support vector machine
TDM	Texturing during moulding

Appendix A

Table A1. Data Quality Report.

Feature	Number of Values	Missing Values	Cardinality	Minimum	1st Quartil
Sliding velocity in mm/s	3990	0	19	1.00	5.00
Cycle	3990	0	11	1.00	4.00
Direction of motion	3990	0	2	−1.00	−1.00
Dimple diameter in µm	3990	0	10	96.51	100.35
Dimple distance in µm	3990	0	10	195.76	243.54
Dimple depth in µm	3990	0	10	7.91	11.41
Real texture density	3990	0	10	0.15	0.20
Friction coefficient	3990	0	3990	0.03	0.08

Feature	Mean	Median	3rd Quartil	Maximum	Standard deviation
Sliding velocity in mm/s	89.21	10.00	100.00	500.00	145.94
Cycle	6.24	6.00	9.00	11.00	3.04
Direction of motion	−0.50	−1.00	1.00	1.00	1.00
Dimple diameter in µm	142.57	147.23	149.23	199.10	34.74
Dimple distance in µm	278.20	292.59	293.60	389.86	48.99
Dimple depth in µm	16.55	16.79	23.32	24.78	5.99
Real texture density	0.26	0.26	0.27	0.45	0.08
Friction coefficient	0.12	0.11	0.16	0.42	0.06

Table A2. Summary of all algorithms and their performance indices within the first model epoch with the full dataset according to Section 5.2 studied by category: Supervised Learning — Regression.

Category	No.	Algorithm	*MSE*	R^2
Linear Regression Models	1	Linear	0.00259	0.27744
	2	Interactions Linear	0.00214	0.40334
	3	Robust Linear	0.00259	0.27707
	4	Stepwise Linear	0.00212	0.40908

Table A2. *Cont.*

Category	No.	Algorithm	*MSE*	R^2
Regression Trees	5	Fine Tree	0.00001	0.99738
	6	Medium Tree	0.00002	0.99337
	7	Coarse Tree	0.00011	0.96963
Support Vector Machines	8	Linear SVM	0.00262	0.26978
	9	Quadratic SVM	0.00133	0.62854
	10	Cubic SVM	0.00146	0.59357
	11	Fine Gaussian SVM	0.00057	0.84057
	12	Medium Gaussian SVM	0.00104	0.71004
	13	Coarse Gaussian SVM	0.00224	0.37614
Gaussian Process Regression Models	14	Squared Exponential	0.00046	0.87305
	15	Matern 5/2	0.00035	0.90343
	16	Exponential	0.00014	0.96152
	17	Rational Quadric	0.00036	0.90069
Kernel Approximation Models	18	SVM Kernel	0.00003	0.99114
	19	Least Squares Kernel Regression	0.00013	0.96501
Ensembles of Trees	20	Boosted Trees	0.00013	0.96412
	21	Bagged Trees	0.00018	0.95081
Neural Networks	22	Narrow Neural Network	0.00015	0.95800
	23	Medium Neural Network	0.00008	0.97772
	24	Wide Neural Network	0.00005	0.98352
	25	Bilayered Neural Network	0.00006	0.98428
	26	Trilayered Neural Network	0.00007	0.98161

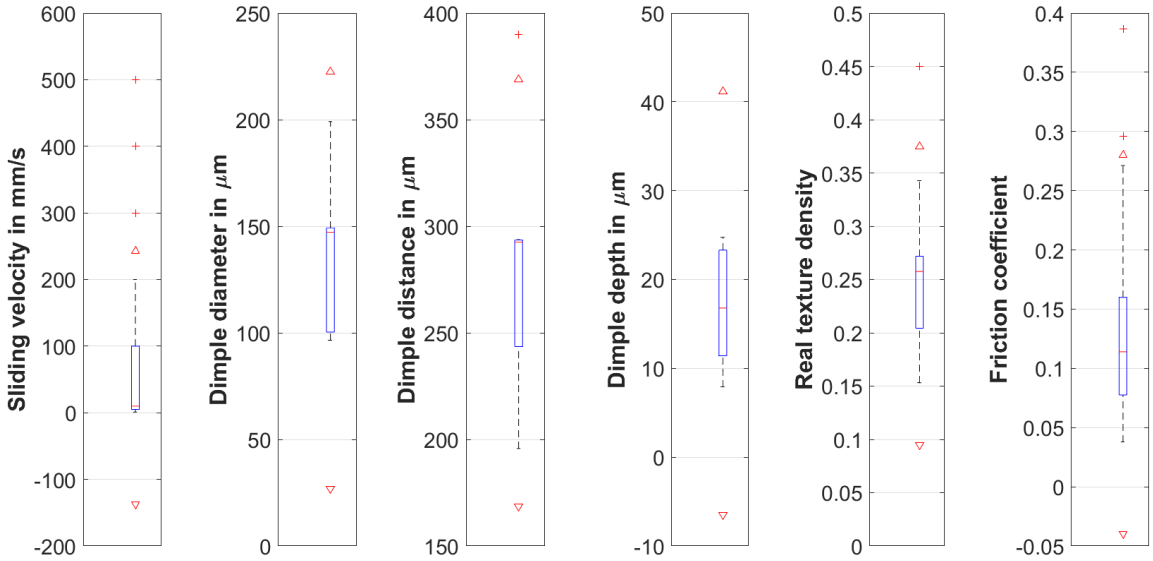

Figure A1. Boxplots of relevant features for visualising IQR. The lower and upper quartile (blue), lower and upper whisker (black), median (red line), lower limit (red downward-pointing triangle) and upper limit of the IQR (red upward-pointing triangles), and outliers (red crosses) are shown. The features cycle and direction of motion are not considered, as they only represent a numerator and the numerical representation of the direction.

References

1. Menezes, P.L.; Nosonovsky, M.; Ingole, S.P.; Kailas, S.V.; Lovell, M.R. (Eds.) *Tribology for Scientists and Engineers*; Springer: Berlin/Heidelberg, Germany, 2013.
2. Holmberg, K.; Erdemir, A. Influence of tribology on global energy consumption, costs and emissions. *Friction* **2017**, *5*, 263–284. [CrossRef]

3. Chandross, M.; Argibay, N. Friction of metals: A review of microstructural evolution and nanoscale phenomena in shearing contacts. *Tribol. Lett.* **2021**, *69*, 119. [CrossRef]
4. Bhagwat, P.; Sista, B.; Vemaganti, K. A computational study of the effects of strain hardening in micro-asperity friction models. *Tribol. Lett.* **2017**, *65*, 154. [CrossRef]
5. Reid, J.V.; Schey, J. A. The effect of surface hardness on friction. *Wear* **1987**, *118*, 113–125. [CrossRef]
6. Rejhon, M.; Lavini, F.; Khosravi, A.; Shestopalov, M.; Kunc, J.; Tosatti, E.; Riedo, E. Relation between interfacial shear and friction force in 2D materials. *Nat. Nanotechnol.* **2022**, *17*, 1280–1287. [CrossRef] [PubMed]
7. Zhou, X.; Liu, Y.; Hu, X.; Fang, L.; Song, Y.; Liu, D.; Luo, J. Influence of elastic property on the friction between atomic force microscope tips and 2D materials. *Nanotechnology* **2020**, *31*, 28. [CrossRef] [PubMed]
8. Farhat, Z.N.; Ding, Y.; Northwood, D.O.; Alpas, A.T. Effect of grain size on friction and wear of nanocrystalline aluminum. *Mater. Sci. Eng.* **1996**, *206*, 302–313. [CrossRef]
9. Penfornis, C.; Jourani, A.; Mazeran, P.-E. Effect of Grain Sizes on the Friction and Wear Behavior of Dual-Phase Microstructures with Similar Macrohardness and Composition. *Coatings* **2023**, *13*, 533. [CrossRef]
10. Kalin, M.; Polajnar, M. The effect of wetting and surface energy on the friction and slip in oil-lubricated contacts. *Tribol. Lett.* **2013**, *52*, 185–194. [CrossRef]
11. Rabinowicz, E. Influence of surface energy on friction and wear phenomena. *J. Appl. Phys.* **1961**, *32*, 1440–1444. [CrossRef]
12. Al-Bender, F.; De Moerlooze, K. On the relationship between normal load and friction force in pre-sliding frictional contacts. Part 1: Theoretical analysis. *Wear* **2010**, *269*, 174–182. [CrossRef]
13. De Moerlooze, K.; Al-Bender, F. On the relationship between normal load and friction force in pre-sliding frictional contacts. Part 2: Experimental investigation. *Wear* **2010**, *269*, 183–189. [CrossRef]
14. Horovistiz, A.; Laranjeira, S.; Davim, J.P. Influence of sliding velocity on the tribological behavior of PA66GF30 and PA66+ MoS2: An analysis of morphology of sliding surface by digital image processing. *Polym. Bull.* **2018**, *75*, 5113–5131. [CrossRef]
15. Tile, P.S.; Thomas, B. Effect of Load, Sliding Velocity, and Reinforcements on Wear Characteristics of Al7075-Based Composite and Nanocomposites Fabricated by Ultrasonic-Assisted Stir-Casting Technique. *Int. J. Met.* **2023**, 1–16. . [CrossRef]
16. Kou, B.; Li, Z.; Li, R.; Wang, Z.; Zhao, X. Influence of external environment parameters on friction coefficient between hoisting-rope and its pads. *AIP Adv.* **2023**, *13*, 6. [CrossRef]
17. Li, P.; Wang, B.; Ji, L.; Li, H.; Chen, L.; Liu, X.; Zhou, H.; Chen, J. Environmental molecular effect on the macroscale friction behaviors of graphene. *Front. Chem.* **2021**, *9*, 679417. [CrossRef] [PubMed]
18. Harsha, A.P.; Wäsche, R. Influence of temperature on friction and wear characteristics of polyaryletherketones and their composites under reciprocating sliding condition. *J. Mater. Eng. Perform.* **2018**, *27*, 5438–5449. [CrossRef]
19. Gropper, D.; Wang, L.; Harvey, T.J. Hydrodynamic lubrication of textured surfaces: A review of modeling techniques and key findings. *Tribol. Int.* **2016**, *94*, 509–529. [CrossRef]
20. Müser, M.H.; Nicola, L. Modeling the surface topography dependence of friction, adhesion, and contact compliance. *MRS Bull.* **2022**, *47*, 1221–1228. [CrossRef]
21. Lu, P.; Wood, R.J. Tribological performance of surface texturing in mechanical applications—A review. *Surf. Topogr. Metrol. Prop.* **2020**, *8*, 043001. [CrossRef]
22. Vishnoi, M.; Kumar, P.; Murtaza, Q. Surface texturing techniques to enhance tribological performance: A review. *Surf. Interfaces* **2021**, *27*, 101463. [CrossRef]
23. Bergseth, E.; Zhu, Y.; Söderberg, A. Study of surface roughness on friction in rolling/sliding contacts: Ball-on-disc versus twin-disc. *Tribol. Lett.* **2020**, *68*, 69. [CrossRef]
24. Ivanović, L.; Vencl, A.; Stojanović, B.; Marković, B. Biomimetics Design for Tribological Applications. *Tribol. Ind.* **2018**, *40*, 448–456. [CrossRef]
25. Grützmacher, P.G.; Profito, F.J.; Rosenkranz, A. Multi-Scale Surface Texturing in Tribology—Current Knowledge and Future Perspectives. *Lubricants* **2019**, *7*, 95. [CrossRef]
26. Martini, A.; Zhu, D.; Wang, Q. Friction reduction in mixed lubrication. *Tribol. Lett.* **2007**, *28*, 139–147. [CrossRef]
27. Brito, F.P.; Miranda, A.S.; Claro, J.C.P.; Teixeira, J.C.; Costa, L.; Fillon, M. The role of lubricant feeding conditions on the performance improvement and friction reduction of journal bearings. *Tribol. Int.* **2014**, *72*, 65–82. [CrossRef]
28. Bobach, L.; Bartel, D.; Beilicke, R.; Mayer, J.; Michaelis, K.; Stahl, K.; Bachmann, S.; Schnagl, J.; Ziegele, H. Reduction in EHL Friction by a DLC Coating. *Tribol. Lett.* **2015**, *60*, 17. [CrossRef]
29. Fukata, M.; Sotani, T.; Motozawa, M. Leakage and friction characteristics at sliding surface of tip seal in scroll compressors. *Int. J. Refrig.* **2021**, *125*, 104–112. [CrossRef]
30. Charitopoulos, A.; Visser, R.; Eling, R.; Papadopoulos, C.I. Design Optimization of an Automotive Turbocharger Thrust Bearing Using a CFD-Based THD Computational Approach. *Lubricants* **2018**, *6*, 21. [CrossRef]
31. Rosenkranz, A.; Costa, H.L.; Baykara, M.Z.; Martini, A. Synergetic effects of surface texturing and solid lubricants to tailor friction and wear—A review. *Tribol. Int.* **2021**, *155*, 106792. [CrossRef]
32. Zhang, K.; Deng, J.; Guo, X.; Sun, L.; Lei, S. Study on the adhesion and tribological behavior of PVD TiAlN coatings with a multi-scale textured substrate surface. *Int. J. Refract. Met. Hard Mater.* **2018**, *72*, 292–305. [CrossRef]
33. Gachot, C.; Rosenkranz, A.; Reinert, L.; Ramos-Moore, E.; Souza, N.; Müser, M.H.; Mücklich, F. Dry Friction Between Laser-Patterned Surfaces: Role of Alignment, Structural Wavelength and Surface Chemistry, *Tribol. Lett.* **2013**, *49*, 193–202. [CrossRef]

34. Erdemir, A. Review of engineered tribological interfaces for improved boundary lubrication. *Tribol. Int.* **2005**, *38*, 249–256. [CrossRef]
35. Schneider, J.; Braun, D.; Greiner, C. Laser Textured Surfaces for Mixed Lubrication: Influence of Aspect Ratio, Textured Area and Dimple Arrangement. *Lubricants* **2017**, *5*, 32. [CrossRef]
36. Marian, M.; Grützmacher, P.; Tremmel, S.; Mücklich, F.; Wartzack, S. Designing surface textures for EHL point-contacts—Transient 3D-simulations, meta-modeling and experimental validation. *Tribol. Int.* **2019**, *137*, 152–163. [CrossRef]
37. Costa, H.L.; Hutchings, I.M. Hydrodynamic lubrication of textured steel surfaces under reciprocating sliding conditions. *Tribol. Int.* **2007**, *40*, 1227–1238. [CrossRef]
38. Prodanov, N.; Gachot, C.; Rosenkranz, A.; Mücklich, F.; Müser, M.H. Contact Mechanics of Laser-Textured Surfaces. *Tribol. Lett.* **2013**, *50*, 41–48. [CrossRef]
39. Rosenkranz, A.; Heib, T.; Gachot, c.; Mücklich, F. Oil film lifetime and wear particle analysis of laser-patterned stainless steel surfaces. *Wear* **2015**, *334–335*, 1–12. [CrossRef]
40. Hsu, C.-J.; Stratmann, A.; Rosenkranz, A.; Gachot, C. Enhanced Growth of ZDDP-Based Tribofilms on Laser-Interference Patterned Cylinder Roller Bearings. *Lubricants* **2017**, *5*, 39. [CrossRef]
41. Kovalchenko, A.; Ajayi, O.; Erdemir, A.; Fenske, G.; Etsion, I. The effect of laser surface texturing on transitions in lubrication regimes during unidirectional sliding contact. *Tribol. Int.* **2005**, *38*, 219–225. [CrossRef]
42. Etsion, I. Modeling of surface texturing in hydrodynamic lubrication. *Friction* **2013**, *1*, 195–209. [CrossRef]
43. Dumont, M.-L.; Lugt, P.M.; Tripp, J.H. Surface feature effects in starved circular EHL contacts. *J. Tribol.* **2002**, *124*, 358–366. [CrossRef]
44. Wang, Z.; Ye, R.; Xiang, J. The performance of textured surface in friction reducing: A review. *Tribol. Int.* **2023**, *177*, 108010. [CrossRef]
45. Gachot, C.; Rosenkranz, A.; Hsu, S.M.; Costa, H.L. A critical assessment of surface texturing for friction and wear improvement. *Wear* **2017**, *372–373*, 21–41. [CrossRef]
46. Chen, K.; Yang, X.; Zhang, Y.; Yang, H.; Lv, G.; Gao, Y. Research progress of improving surface friction properties by surface texture technology. *Int. J. Adv. Manuf. Technol.* **2021**, *116*, 2797–2821. [CrossRef]
47. Marian, M.; Tremmel, S. Current trends and applications of machine learning in tribology—A review. *Lubricants* **2021**, *9*, 86. [CrossRef]
48. Paturi, U.M.R.; Palakurthy, S.T.; Reddy, N.S. The Role of Machine Learning in Tribology: A Systematic Review. *Arch. Comput. Methods Eng.* **2022**, *30*, 1345–1397. [CrossRef]
49. Sterkenburg, F.S.; Grünwald, P.D. The no-free-lunch theorems of supervised learning. *Synthese* **2021**, *199*, 9979–10015. [CrossRef]
50. Kelleher, J.D.; Macnamee, B.; D'Arcy, A. *Fundamentals of Machine Learning for Predictive Data Analytics: Algorithms, Worked Examples, and Case Studies*; The MIT Press: Cambridge, MA, USA; London, UK, 2015.
51. Zambrano, V.; Brase, M.; Hernandez-Gascon, B.; Wangenheim, M.; Gracia, L.; Viejo, I.; Izquierdo, S.; Valdes, J. A Digital Twin for Friction Prediction in Dynamic Rubber Applications with Surface Textures. *Lubricants* **2021**, *9*, 57. [CrossRef]
52. Klüber Lubrication München GmbH. Centoplex 2 EP—Product Information. Available online: https://www.klueber.com/de/de/produkte-service/produkte/centoplex-2-ep/9971/ (accessed on 26 October 2023).
53. Albon, C. *Machine Learning Kochbuch: Praktische Lösungen mit Python: Von der Vorverarbeitung der Daten bis zum Deep Learning*, 1st ed.; O'Reilly: Heidelberg, Germany, 2019.
54. Tukey, J.W. *Exploratory Data Analysis*; Book Addison-Wesley: Reading, PA, USA, 1977.
55. Falk, M.; Marohn, F.; Becker, R. *Angewandte Statistik MIT SAS: Eine Einführung*; Springer: Berlin/Heidelberg, Germany, 1995.
56. Wilmott, P. *Grundkurs Machine Learning*; Rheinwerk Computing: Bonn, Germany, 2020.
57. James, G.; Witten, D.; Hastie, T.; Tibshirani, R.; Taylor, J. *An Introduction to Statistical Learning*; Springer: Berlin/Heidelberg, Germany, 2023.
58. Fowell, M.; Olver, A.V.; Gosman, A.D.; Spikes, H.A.; Pegg, I. Entrainment and inlet suction: Two mechanisms of hydrodynamic lubrication in textured bearings. *J. Tribol.* **2007**, *2*, 336–347. [CrossRef]
59. Hamilton, D.B.; Walowit, J.A.; Allen, C.M. A theory of lubrication by microirregularities. *J. Basic Eng.* **1966**, *88*, 177–185. [CrossRef]
60. Hsu, S.M.; Jing, Y.; Zhao, F. Self-adaptive surface texture design for friction reduction across the lubrication regimes. *Surf. Topogr. Metrol. Prop.* **2016**, *4*, 014004. [CrossRef]
61. Olver, A.V.; Fowell, M.T.; Spikes, H.A.; Pegg, I.G. 'Inlet suction', a load support mechanism in non-convergent, pocketed, hydrodynamic bearings. *Proc. Inst. Mech. Eng. Part J Eng. Tribol.* **2006**, *220*, 105–108. [CrossRef]
62. Tang, Z.; Liu, X.; Liu, K.; Pegg, I.G. Effect of surface texture on the frictional properties of grease lubricated spherical plain bearings under reciprocating swing conditions. *Proc. Inst. Mech. Eng. Part J Eng. Tribol.* **2017**, *231*, 125–135. [CrossRef]
63. Ahmed, A.; Masjuki, H.H.; Varman, M.; Kalam, M.A.; Habibullah, M.; AL Mahmud, K.A. An overview of geometrical parameters of surface texturing for piston/cylinder assembly and mechanical seals. *Meccanica* **2016**, *51*, 9–23. [CrossRef]
64. Vencl, A.; Ivanovic, L.; Stojanovic, B.; Zadorozhnaya, E.; Miladinovic, S.; Svodoba, B. Surface Texturing for Tribological Applications: A Review. In Proceedings of the 16th International Conference on Tribology, Kragujevac, Serbia, 15–17 May 2019.
65. Wu, Z.; Bao, H.; Xing, Y.; Liu, L. Tribological characteristics and advanced processing methods of textured surfaces: A review. *Int. J. Adv. Manuf. Technol.* **2021**, *114*, 1241–1277. [CrossRef]